International Forum on Aeroelasticity and Structural Dynamics
IFASD 2017
25-28 June 2017 Como, Italy

EXTENSION OF THE CONTINUOUS TIME UNSTEADY VORTEX LATTICE METHOD FOR ARBITRARY MOTION, CONTROL SURFACE DEFLECTION AND INDUCED DRAG CALCULATION

Simon Binder[1], **Andreas Wildschek**[2], **Roeland De Breuker**[3]

[1]Airbus Group Innovations
81663 Munich, Germany
simon.binder@airbus.com

[2]Airbus Group Innovations
81663 Munich, Germany

[3]Delft University of Technology
Kluyverweg 1, 2629 HS, Delft, Netherlands

Keywords: unsteady aerodynamics, continuous time model, state space model, unsteady induced drag, unsteady vortex lattice method

Abstract: In this paper a continuous time state space aerodynamic model is extended for accepting arbitrary motion, control surface deflection and gust velocities as inputs. Equations for formulating the inner state equation are outlined first followed by the numerical description of the boundary condition. The force calculation is presented using an unsteady form of the Kutta-Joukowski theorem enabling the method of unsteady induced drag prediction. Methods for linearization are presented. The resulting model inputs are motion, control surface deflection and gust velocities and accelerations while the system outputs are panel forces. To validate the modeling approach, comparisons to analytical methods are carried out for various oscillatory motions. Besides integrated coefficients for vertical force, drag, pitching moment and hingemoment, comparisons for unsteady pressure distributions are carried out. The comparisons indicate good agreement for a large range of reduced frequencies. The influence of wake truncation distance and discretization is discussed. Because of its time-domain formulation, the model is especially suitable for efficient aerodynamic loads analysis within aeroelastic modeling, analysis and optimization frameworks for preliminary aircraft design.

1 INTRODUCTION

The assessment of aircraft flight dynamics, i.e. the analysis of stability and performance, requires besides others the modeling of the aerodynamic forces. Within conceptual and preliminary design, high turn-around times are necessary for efficient multidisciplinary design optimization. Therefore, potential flow methods for predicting aerodynamic forces have been commonly used in the past because of their relatively low computational costs. Ambitious goals regarding fuel-efficiency drive the development of aircraft towards concepts with reduced structural weight and thus increased structural flexibility making static and dynamic aeroelastic effects non-negligible in the early design stages of aircraft. Thus, accurate modeling and prediction of the unsteady aerodynamics is of great importance.

1.1 Background

Kier [1] described and collected different unsteady aerodynamic modeling approaches. The most important models to name are the doublet lattice method (DLM), strip theory and the unsteady vortex lattice method (UVLM). Advantages of the UVLM and their possible applications have been described by Murua et al. [2]. One of the most important advantages is the capability of modeling nonlinear effects such as deformed wake shapes. Hall [3] described the UVLM as a discrete time state space model formulation. A formulation of the UVLM in continuous time has been first presented by Gologan and Schneider [4]. Mauermann used the results for the development of a novel approach for flexible aircraft modeling [5]. Mohammadi-Amin et al. [6] also developed a continuous time state space aerodynamic model based on the boundary element method in order to overcome disadvantages of discrete models (e.g. fixed time step) for nonlinear analysis and aeroervoelastic optimization. Their description includes a special treatment of the flow tangency condition at the trailing edge which differs from the formulation of Gologan et al. [4]. Werter et al. [7] used those results to formulate the UVLM in a continuous time state space description. Instead of using constant strength doublet panels, vortex ring elements have been used. Arbitrary wing geometries as well as cambered surfaces can be modeled with this approach. The formulation of Werter et al. [7] lacks arbitrary inputs like three dimensional rigid body motion and gusts. Also the equations are linearized from the beginning which limits the method to lift calculation for small angle of attack perturbations around a reference point.

1.2 Goal of the Present Paper

In this paper, the formulation by Werter et al. [7] is extended for accepting arbitrary motion, control surface deflections and panel gust velocities as inputs. The resulting model shall be used in dAEDalus, a nonlinear aeroelastic flight simulation and preliminary aircraft design framework [8]. The formulation is further extended to describe three dimensional forces on the panels. In order to validate the overall implementation, a linearized version of the resulting nonlinear model is first used to calculate unsteady derivatives as well as unsteady pressure distributions for various motions including unsteady flap oscillations which are then compared to analytical solutions. The nonlinear model is then used to calculate the unsteady drag of plunging and pitching motion followed by a comparison to analytical solutions.

2 MODELING OF UNSTEADY AERODYNAMICS

The UVLM is based on potential flow theory. With the assumption of irrotational and incompressible flow, the governing equation of potential flow methods reduces to the Laplace equation. Due to the linearity of the Laplace equation, the flow problem can be stated and solved by a superposition of fundamental solutions for which analytical solutions of the flowfield exist. While the DLM is using doublets (source-sink pair) the fundamental solution of choice in the UVLM is the closed, constant strength vortex ring. In order to model aircraft configurations to solve the flowfield with potential flow methods, the lifting surfaces are discretized by panels (see Fig. 1). In the UVLM also the wake is discretized using panels. At each of the bound panels, a vortex ring is constructed with it's leading edge segment placed at the one-quarter chord line of the panel (see Fig. 1 A). Vortex rings in the wake are placed in a way that they coincide with the panels' edges (see Fig. 1 B). To account for camber, twist and other 3D effects, the bound panels are arranged on the mean surface (between top and bottom skin) of the wings. The position of the wake panels is given by the trajectory of the lifting surface as well as the

flowfield behind the wing. The wake panels are so to say shed into the wake at every time step and from that point on free floating in the flow field (force free wake).

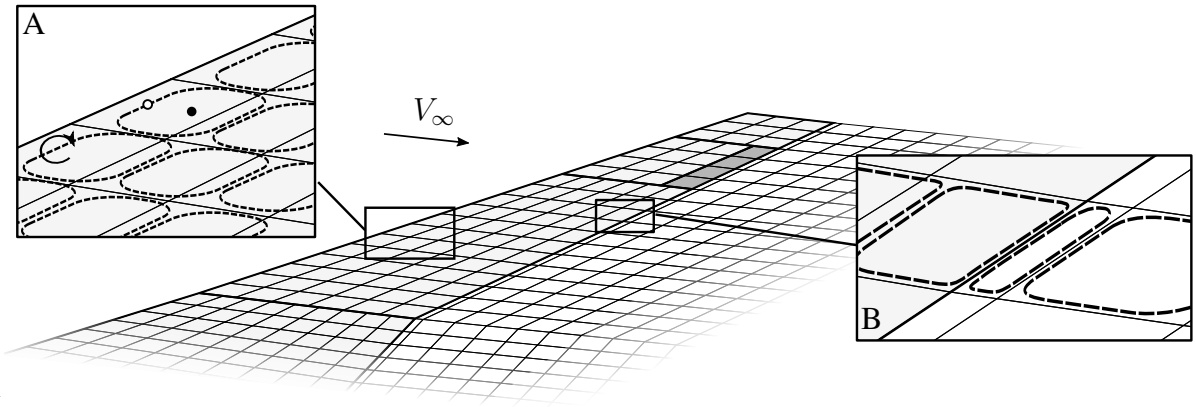

Figure 1: Discretization of a wing surface (light gray panels) and wake (white panels) in the unsteady vortex lattice method. Control surface panels are highlighted in dark gray. A: Vortex rings with collocation points (•) and force application points (○); B: Arrangement of vortex rings at the trailing edge and in the wake.

The solving procedure of the classical, time-stepping UVLM is as follows. For the determination of the strengths of all vortex rings $\vec{\Gamma}$ (unknowns) at time $T = t_1$, the same number of equations as panels is needed. One set of equations is obtained by introducing so called boundary conditions stating that there may be no flow penetrating the wings surface (also called non-penetration condition or zero normal-flow condition). In the UVLM, this non-penetration condition is fulfilled at the center of the vortex rings, i.e. the three-quarter chord of the panels. The vortex-ring induced velocity at those collocation points can be calculated with the influence coefficients which in turn are calculated from the spatial distribution of vortex-rings and collocation points. Another set of equations is obtained by the fulfillment of the Kutta condition which states that no circulation may exist at the wings trailing edge. The remaining required equations are put up by the assumption that the vorticity of a wake vortex ring does not change or changes with a known rate once being shed into the wake. Thus, the vorticity of the wake panels is known from solutions of previous time steps ($T < t_1$) or initial conditions. Knowing the vorticity of each vortex-ring, the forces at every panel can be calculated using the Kutta-Joukowski theorem. Afterwards, the procedure is repeated until solutions at all required time steps are found. For more details of the UVLM in general, the reader is referred to [9].

2.1 Continuous Time Unsteady Vortex Lattice Method

Starting point for the proposed work is the following 3 governing equations of the UVLM describing the boundary condition or normal-wash ($\vec{b}$) on the bound panels, the Kutta condition which states that no circulation Γ may exist at the trailing edge ($\Gamma_{\text{TE}} = 0$), and the transport of vorticity within the wake (as outlined by Werter et al. [7]):

$$\text{Boundary Condition:} \qquad \mathbf{A_1}\vec{\Gamma}^t = \vec{b}^t \tag{1}$$

$$\text{Kutta Condition:} \qquad \mathbf{A_2}\vec{\Gamma}^t = 0 \tag{2}$$

$$\text{Wake Transport Condition:} \qquad \mathbf{A_3}\vec{\Gamma}^t = \mathbf{A_4}\vec{\Gamma}^{t-1} \tag{3}$$

In this equation the superscript t denotes the current time-step, and $t-1$ the previous time-step. The matrix $\mathbf{A_1}$ contains the influence coefficients. $\mathbf{A_2}$ links the vorticity of the first row of the

wake to the rest of the wake. $\mathbf{A_3}$ and $\mathbf{A_4}$ describe the vorticity transport within the wake.
For the continuous time formulation, the vector of vorticities $\vec{\Gamma}$ is first split into three parts. Vorticities of panels on the wings surface ($\vec{\Gamma}_\mathrm{b}$), vorticities of the first row in the wake ($\vec{\Gamma}_\mathrm{w0}$, smaller panels in Fig. 1 B) and the remaining vorticities of the wake ($\vec{\Gamma}_\mathrm{w}$). Using a forward Euler discretization in time for the wake transport equation Werter [7] obtains the following equations:

$$\text{Boundary Condition:} \qquad 0 = \mathbf{K_1}\vec{\Gamma}_\mathrm{b} + \mathbf{K_2}\vec{\Gamma}_\mathrm{w0} + \mathbf{K_3}\vec{\Gamma}_\mathrm{w} - \vec{b} \tag{4}$$

$$\text{Kutta Condition:} \qquad 0 = \mathbf{K_4}\vec{\Gamma}_\mathrm{b} + \mathbf{K_5}\vec{\Gamma}_\mathrm{w0} \tag{5}$$

$$\text{Wake Transport Condition:} \qquad \dot{\vec{\Gamma}}_\mathrm{w} = \mathbf{K_6}\vec{\Gamma}_\mathrm{w} + \mathbf{K_7}\vec{\Gamma}_\mathrm{w0} \tag{6}$$

Note that all equations are now written at time t. The formulation is thus not dependent on previous times anymore (continuous time formulation). By defining $\vec{\Gamma}_\mathrm{w}$ as state variable and inserting Eq. (4) and (5) into (6), a linear state equation can be obtained:

$$\dot{\vec{\Gamma}}_\mathrm{w} = \underbrace{(\mathbf{K_6} + \mathbf{K_7}(\mathbf{K_5} - \mathbf{K_4}{\mathbf{K_1}}^{-1}\mathbf{K_2})^{-1}\mathbf{K_4}{\mathbf{K_1}}^{-1}\mathbf{K_3})}_{\mathbf{K_8}}\vec{\Gamma}_\mathrm{w} \tag{7}$$

$$- \underbrace{\mathbf{K_7}(\mathbf{K_5} - \mathbf{K_4}{\mathbf{K_1}}^{-1}\mathbf{K_2})^{-1}\mathbf{K_4}{\mathbf{K_1}}^{-1}}_{\mathbf{K_9}}\vec{b} \tag{8}$$

$$\dot{\vec{\Gamma}}_\mathrm{w} = \mathbf{K_8}\vec{\Gamma}_\mathrm{w} + \mathbf{K_9}\vec{b} \tag{9}$$

2.2 Input Transformation

Werter et al. express the flow tangency condition $\vec{b}$ as a function of the local angle of attack of the panels α_i. Furthermore the boundary condition is linearized yielding the expression [7]:

$$\vec{b}_i = |\vec{V}_\infty| \begin{bmatrix} 0 \\ 0 \\ \alpha_i \end{bmatrix} \cdot \vec{n}_i \tag{10}$$

With $\vec{n}_i$ being the normal vector of the panel i and $\vec{V}_\infty$ the freestream velocity. A more general expression of the boundary condition is:

$$\vec{b}_i = \vec{V}_i \cdot \vec{n}_i \tag{11}$$

To account for control surface deflection, the normal vectors of control surface panels have to be formulated in dependency of the deflection angle. This is done using the Rodrigues rotation formula [10]:

$$\vec{n}_i = \mathbf{T_{\delta,i}}\vec{n}_{0,i} = [\mathbf{I} + \sin(\delta_j)\mathbf{K_j} + (1 - \cos(\delta_j)){\mathbf{K_j}}^2)]\vec{n}_{0,i} \tag{12}$$

with $\mathbf{K_j}$ being the skew symmetric matrix of the axis direction vector $\vec{k}_j$ of the respective control surface j, its deflection angle δ_j and the normal vector at zero deflection $\vec{n}_i$ (see Fig. 2).

To account for arbitrary motion, control surface deflection and gust velocities, the total velocity $\vec{V}_i$ at the collocation point of panel i is split in four parts:

$$\vec{V}_i = \vec{V}_\infty + \vec{V}_{\omega_\infty,i} + \vec{V}_{\dot{\delta}_j} + \vec{V}_{g,i} \tag{13}$$

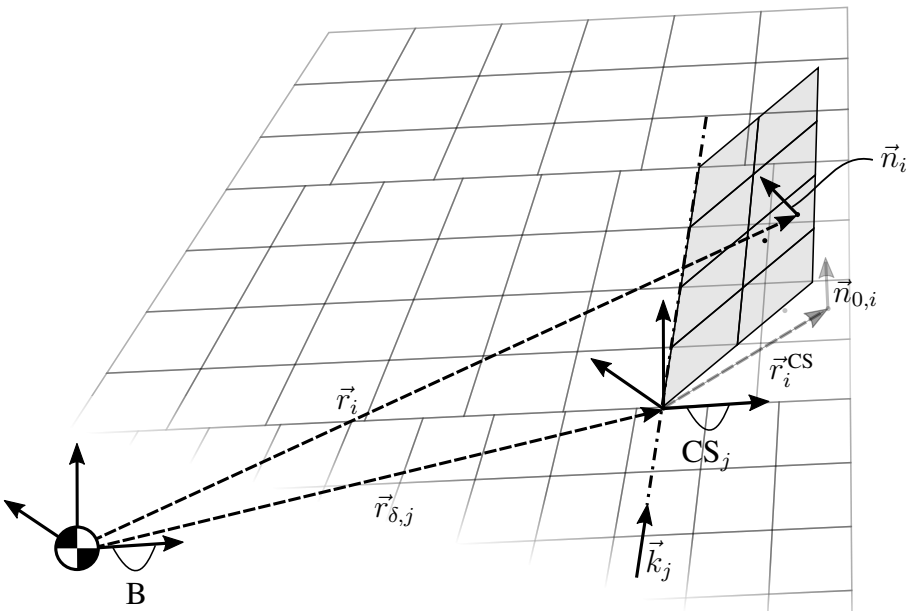

Figure 2: Description of the kinematics involved in control surface deflection: Rotation of the normalvector of panel i ($\vec{n}_{0,i} \rightarrow \vec{n}_i$) around the hinge axis $\vec{k}_j$ and the resulting positioning vector of the collocation point $\vec{r}_{\delta,j} + \vec{r}_i^{\,\mathrm{CS}} \rightarrow \vec{r}_i$

In which $\vec{V}_{\omega_\infty,i}$ is the local induced velocity due to rotations in the freestream flow field caused by e.g. body rotation, $\vec{V}_{\dot{\delta}_j}$ the velocity due to control surface deflection rate and $\vec{V}_{g,i}$ the local gust induced velocity. The induced velocity due to rotations is described by:

$$\vec{V}_{\omega_\infty,i} = \vec{\omega}_\infty \times \vec{r}_i \tag{14}$$

With $\vec{\omega}_\infty$ being the vector of rotations in the freestream and $\vec{r}_i$ being the distance from the panel's collocation point to the rotational center (e.g. body rotational center). For control surface panels, this distance changes with the deflection of the control surface (see Fig. 2):

$$\vec{r}_i = (\vec{r}_{\delta,j} + \mathbf{T}_{\boldsymbol{\delta,j}} \vec{r}_i^{\,\mathrm{CS}}) \tag{15}$$

in which $\vec{r}_{\delta,j}$ is the vector from the center of rotation to the origin of the control surface coordinate system CS_j and $\vec{r}_i^{\,\mathrm{CS}}$ describes the location of the collocation point in the CS_j frame.
The velocity influence due to control surface deflection rates $\vec{V}_{\dot{\delta},i}$ is calculated as:

$$\vec{V}_{\dot{\delta},i} = \dot{\mathbf{T}}_{\boldsymbol{\delta,j}} \vec{r}_i^{\,\mathrm{CS}} \tag{16}$$

with the time derivative of the Rodrigues rotation matrix $\dot{\mathbf{T}}_{\boldsymbol{\delta,j}}$:

$$\dot{\mathbf{T}}_{\boldsymbol{\delta,j}} = \dot{\delta}_j(\cos(\delta_j)\mathbf{K}_{\boldsymbol{j}} + \sin(\delta_j)\mathbf{K}_{\boldsymbol{j}}{}^2) \tag{17}$$

The gust velocities $\vec{V}_{g,i}$ are assumed to be known. In total Eq. (11) can be expressed as the nonlinear function:

$$b_i = (\vec{V}_\infty + \vec{\omega}_\infty \times (\vec{r}_{\delta,j} + \mathbf{T}_{\boldsymbol{\delta,j}} \vec{r}_i^{\,\mathrm{CS}}) + \dot{\mathbf{T}}_{\boldsymbol{\delta,j}} \vec{r}_i^{\,\mathrm{CS}} + \vec{V}_{g,i}) \cdot \mathbf{T}_{\boldsymbol{\delta,i}} \vec{n}_{0,i} \tag{18}$$

A linearized formulation of the above equation can be found assuming small control surface deflections. In this case, the distance of the rotational center and the collocation point $\vec{r}_i$ does not change with control surface deflections. Furthermore it can be assumed that control surface deflection only has an influence on the boundary condition due to freestream velocity at the linearization point. Linearizing for a speed of $|\vec{V}_\infty| = V_{\text{lin}}$, Eq. (18) gets:

$$b_i = (\vec{V}_\infty + \vec{\omega}_\infty \times \vec{r}_{\delta,i} + \dot{\mathbf{T}}_{\boldsymbol{\delta,j}} \vec{r}_i^{\,\text{CS}} + \vec{V}_{g,i}) \cdot \vec{n}_{0,i} + V_{\text{lin}} \mathbf{T}_{\boldsymbol{\delta,i}} \vec{n}_{0,i} \tag{19}$$

This linearized formulation is valid for small perturbations around V_{lin}. The boundary condition of all panels may also be written as a linear function of the form:

$$\vec{b} = f(\vec{V}_\infty, \vec{\omega}_\infty, \vec{\delta}, \dot{\vec{\delta}}, \vec{V}_g) \tag{20}$$

With $\vec{\delta}$ and $\dot{\vec{\delta}}$ being the vector of control surface deflections and rates. As later necessary, it should be mentioned that f is a differentiable function:

$$\dot{\vec{b}} = f(\vec{V}_\infty, \dot{\vec{V}}_\infty, \vec{\omega}_\infty, \dot{\vec{\omega}}_\infty, \vec{\delta}, \dot{\vec{\delta}}, \ddot{\vec{\delta}}, \vec{V}_g, \dot{\vec{V}}_g) \tag{21}$$

2.3 Nonlinear Force Computation

In this work, the aerodynamic forces are calculated using an unsteady vector form of the Kutta-Joukowski theorem as outlined by Drela [11]. The unsteady force contribution from an incremental segment of vorticity (described by the vector $\vec{s}$) in three dimensions is [12]:

$$\vec{F} = \rho\Gamma(\vec{V}_\text{s} \times \vec{s}) + \rho\dot{\Gamma}c(\vec{\hat{V}}_\text{s} \times \vec{\hat{s}}) \tag{22}$$

where $\vec{V}_\text{s}$ describes the flow velocity at the center of the segment, and c the chord of the lifting profile. Assuming the unsteady force component acts normal on each vortex ring and the normal vector does not change with control surface deflection, the total force contribution from each panel in three dimensions gets [13]:

$$\vec{F}_i = \rho\Gamma_{\text{b,eff},i}(\vec{V}_{\text{s},i} \times \vec{s}_i) + \rho\dot{\Gamma}_{\text{b,eff},i} A_i \vec{n}_{0,i} \tag{23}$$

Here A_i is the area of the panel and $\Gamma_{\text{b,eff},i}$ describes the effective vorticity of the bound panel i which is defined as (see Fig. 3):

$$\begin{aligned} &\text{LE-Panel:} && \Gamma_{\text{b,eff},i} = \Gamma_{\text{b},i} \\ &\text{Other:} && \Gamma_{\text{b,eff},i} = \Gamma_{\text{b},i} - \Gamma_{\text{b},i-1} \end{aligned} \tag{24}$$

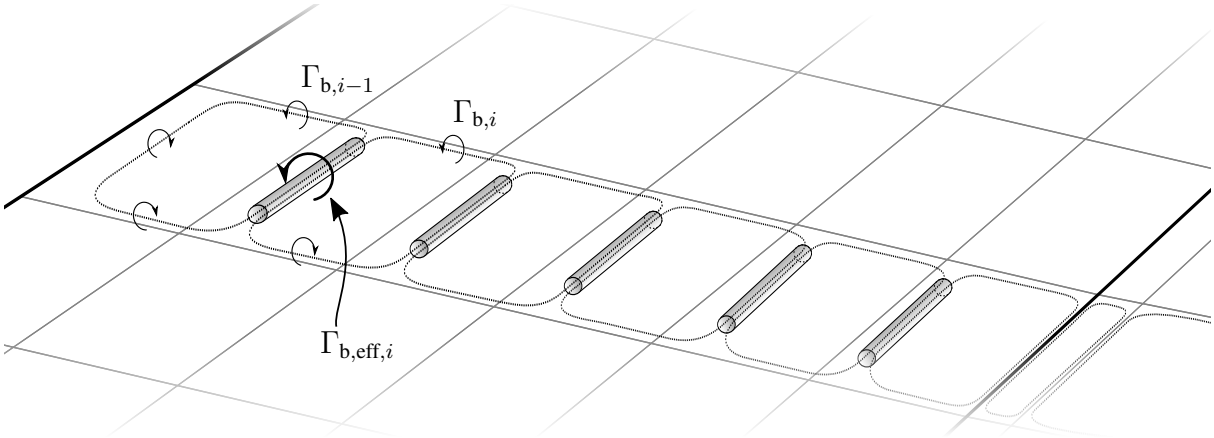

Figure 3: Determination of the effective vorticity $\Gamma_{\mathrm{b,eff},i}$ of a wing surface bound panel i by the summation of vorticities of adjacent vortex rings.

The vector of vorticities of the bound panels $\vec{\Gamma}_{\mathrm{b}}$ can be expressed as a function of wake vorticities $\vec{\Gamma}_{\mathrm{w0}}$ and vector of boundary conditions $\vec{b}$ by substitution of Eq. (5) in (4):

$$\vec{\Gamma}_{\mathrm{b}} = \underbrace{(\mathbf{K_2}\mathbf{K_5}^{-1}\mathbf{K_4} - \mathbf{K_1})^{-1}\mathbf{K_3}}_{\mathbf{L_3}}\vec{\Gamma}_{\mathrm{w}} - \underbrace{\mathbf{K_2}\mathbf{K_5}^{-1}\mathbf{K_4} - \mathbf{K_1})^{-1}}_{\mathbf{L_4}}\vec{b} \tag{25}$$

$$= \mathbf{L_3}\vec{\Gamma}_{\mathrm{w}} - \mathbf{L_4}\vec{b} \tag{26}$$

Similar, the effective derivative of the vorticity needed in Eq. (23) of the panel $\dot{\Gamma}_{\mathrm{b,eff},i}$ is calculated as [14]:

$$\begin{aligned} &\text{LE-Panel:} && \dot{\Gamma}_{\mathrm{b,eff},i} = \frac{1}{2}\dot{\Gamma}_{\mathrm{b},i} \\ &\text{Other:} && \dot{\Gamma}_{\mathrm{b,eff},i} = \frac{1}{2}(\dot{\Gamma}_{\mathrm{b},i} + \dot{\Gamma}_{\mathrm{b},i-1}) \end{aligned} \tag{27}$$

The derivatives of the bound panel vorticities can be calculated by deriving Eq. (26) and inserting the state equation (Eq. (9)):

$$\dot{\vec{\Gamma}}_{\mathrm{b}} = \mathbf{L_3}\dot{\vec{\Gamma}}_{\mathrm{w}} - \mathbf{L_4}\dot{\vec{b}} \tag{28}$$

$$= \mathbf{L_3}(\mathbf{K_8}\vec{\Gamma}_{\mathrm{w}} + \mathbf{K_9}\vec{b}) - \mathbf{L_4}\dot{\vec{b}} \tag{29}$$

$$= \underbrace{\mathbf{L_3}\mathbf{K_8}}_{\mathbf{L_5}}\vec{\Gamma}_{\mathrm{w}} + \underbrace{\mathbf{L_4}\mathbf{K_9}}_{\mathbf{L_6}}\vec{b} - \mathbf{L_4}\dot{\vec{b}} \tag{30}$$

$$= \mathbf{L_5}\vec{\Gamma}_{\mathrm{w}} + \mathbf{L_6}\vec{b} - \mathbf{L_4}\dot{\vec{b}} \tag{31}$$

Eq. (23) furthermore contains the total velocities at the force vector application points, i.e. the 1/4 chord points of the panels, which is calculated as:

$$\vec{V}_{\mathrm{s,i}} = \vec{V}_{\mathrm{s},\infty,i} + \vec{V}_{\mathrm{s,ind,i}} \tag{32}$$

The velocity resulting from rigid body motion and disturbances like gusts $\vec{V}_{\mathrm{s},\infty,i}$ can be determined similarly as the total velocity at the collocation points $\vec{V}_i$ in Eq. (13):

$$\vec{V}_{\mathrm{s},\infty,i} = (\vec{V}_\infty + \vec{\omega}_\infty \times (\vec{r}_{\delta,j} + \mathbf{T_{\delta,j}}\vec{r}^{\,\mathrm{CS}}_{s,i}) + \dot{\mathbf{T}}_{\boldsymbol{\delta,j}}\vec{r}^{\,\mathrm{CS}}_{s,i} + \vec{V}_{g,s,i}) \tag{33}$$

The locally induced velocity at the force vector application points $\vec{V}_{\text{s,ind},i}$ in x-,y- and z-direction in Eq. (32) can be calculated with an additional set of influence coefficients:

$$\vec{V}_{\text{s,ind}} = \begin{bmatrix} \vec{V}_{\text{s,ind},1,x} \\ \vec{V}_{\text{s,ind},1,y} \\ \vec{V}_{\text{s,ind},1,z} \\ \vdots \\ \vec{V}_{\text{s,ind},n,x} \\ \vec{V}_{\text{s,ind},n,y} \\ \vec{V}_{\text{s,ind},n,z} \end{bmatrix} = \mathbf{K_{10}}\vec{\Gamma}_{\text{b}} + \mathbf{K_{11}}\vec{\Gamma}_{\text{w}} + \mathbf{K_{12}}\vec{\Gamma}_{\text{w0}} \tag{34}$$

The required vorticites of the first row in the wake $\vec{\Gamma}_{\text{w0}}$ can be expressed as a function of wake vorticities $\vec{\Gamma}_{\text{w}}$ and boundary condition $\vec{\Gamma}_{\text{b}}$ by substitution of Eq. (4) in (5):

$$\vec{\Gamma}_{\text{w0}} = \underbrace{(\mathbf{K_5} - \mathbf{K_4}\mathbf{K_1}^{-1}\mathbf{K_2})^{-1}\mathbf{K_4}\mathbf{K_1}^{-1}\mathbf{K_3}}_{\mathbf{L_7}}\vec{\Gamma}_{\text{w}} - \underbrace{(\mathbf{K_5} - \mathbf{K_4}\mathbf{K_1}^{-1}\mathbf{K_2})^{-1}\mathbf{K_4}\mathbf{K_1}^{-1}}_{\mathbf{L_8}}\vec{b} \tag{35}$$

$$= \mathbf{L_7}\vec{\Gamma}_{\text{w}} - \mathbf{L_8}\vec{b} \tag{36}$$

By substituting Eq. (24), (27) and (32) in Eq. (23), the three-dimensional force of all panels can be stated as a nonlinear function of the following form:

$$\vec{F} = \begin{bmatrix} \vec{F}_{1,x} \\ \vec{F}_{1,y} \\ \vec{F}_{1,z} \\ \vdots \\ \vec{F}_{n,x} \\ \vec{F}_{n,y} \\ \vec{F}_{n,z} \end{bmatrix} = f(\vec{\Gamma}_{\text{w}}, \vec{V}_{\infty}, \dot{\vec{V}}_{\infty}, \vec{\omega}_{\infty}, \dot{\vec{\omega}}_{\infty}, \vec{\delta}, \dot{\vec{\delta}}, \ddot{\vec{\delta}}, \vec{V}_g, \dot{\vec{V}}_g) \tag{37}$$

A linearization of Eq, (23) can be found by the assumption that the induced velocity at the vortex segment is negligible ($\vec{V}_{\text{s,ind,i}} \approx 0$) and the freestream velocity at the segment center is the reference condition ($\vec{V}_{\text{s},\infty,i} \approx \vec{V}_{\infty,\text{lin}}$):

$$\vec{F}_i = \rho\Gamma_{\text{b,eff},i}(\vec{V}_{\infty,\text{lin}} \times \vec{s}_i) + \rho\dot{\Gamma}_{\text{b,eff},i}A_i\vec{n}_{0,i} \tag{38}$$

2.4 Overall State Space Model Integration

To realize the overall system, the wake vorticities are chosen as states ($\vec{x} = \vec{\Gamma}_{\text{w}}$). The inputs to the system are freestream velocity, freestream rotation, control surface deflections, gust velocities and their derivatives ($\vec{u} = [\vec{V}_{\infty}, \dot{\vec{V}}_{\infty}, \vec{\omega}_{\infty}, \dot{\vec{\omega}}_{\infty}, \vec{\delta}, \dot{\vec{\delta}}, \ddot{\vec{\delta}}, \vec{V}_g, \dot{\vec{V}}_g]^T$). The output of the system is formed by the three-dimensional panel forces ($\vec{y} = \vec{F}$). A nonlinear state space model can be described by using the state equation (Eq. (9)), the linearized formulation of the boundary condition (Eq. (20) & (21)) and the nonlinear form of the force computation (Eq. (37)):

$$\dot{\vec{x}} = \mathbf{A}\vec{x} + \mathbf{B}\vec{u} \tag{39}$$

$$\vec{y} = f(\vec{x}, \vec{u}) \tag{40}$$

A second model is realized using the linearized version of the force computation described in Eq. (38). With this equation, the overall system gets linear and can be realized in the form of a general linear state space system:

$$\dot{\vec{x}} = \mathbf{A}\vec{x} + \mathbf{B}\vec{u} \tag{41}$$

$$\vec{y} = \mathbf{C}\vec{x} + \mathbf{D}\vec{u} \tag{42}$$

3 RESULTS AND DISCUSSION

In order to verify the proposed modeling approach, the response due to various unsteady motions are investigated in the following.

In this chapter, first a comparison of the linearized model (second model) with analytical solutions from Theodorsen [15] and Kier [16] are presented in order to validate the overall implementation of the continuous time unsteady vortex lattice method. A grid independence study is presented identifying the minimum chordwise discretization needed. Furthermore, the influence of the truncation distance of the wake is discussed. The nonlinear force computation (second model) is then compared to analytical solutions described by Garrick [17]. All the analytical methods used for comparison are formulated for 2D flat plate airfoil section.

3.1 Performance Evaluation of the Linearized Model

Theodorsen analyses the problem of unsteady aerodynamics of an oscillating airfoil-aileron combination of three degrees of freedom (vertical/plunge, pitch and aileron/flap degree of freedom). The solution consists of unsteady integrated vertical force, pitching moment and flap hinge moment coefficients (C_Z, C_M and C_H) for harmonic plunging, pitching and control surface motion in dependency of the reduced frequency ($k = \frac{\omega c}{2V_\infty}$; nondimensionalized frequency), the pitching axis location x_p and the hingeline position x_h [15].

To mimic the 2D problem with the 3D implementation of the UVLM, a wing with an extremely large aspect ratio of $AR = 5000$ is modeled. The wake is modelled with a high length of 20 chord-lengths. Furthermore, the pitching axis is placed at the one quarter chord axis ($x_p = 0.25c$), the flap hingeline is positioned at the three quarter chord location ($x_h = 0.75c$). Unless otherwise stated, the airfoil is discretized using 32 panels in chordwise direction and 8 panels in spanwise direction. The discretization of the wake is chosen accordingly meaning that the length and width of wake panels is the same as the length and width of the bound panels which is necessary for the validity of the wake transport equation.

3.1.1 Frequency Response

The standard method of characterizing linear system dynamics is using the frequency response as a quantitative measure. To compare the UVLM to the results from Theodorsen [15], the error in magnitude and phase is calculated. The magnitude error is defined as difference between the UVLM and Theodorsen magnitude data normed to the Theodorsen magnitude. The phase error is defined as the difference between the UVLM and Theodorsen phase data normed to $\frac{\pi}{2}$.

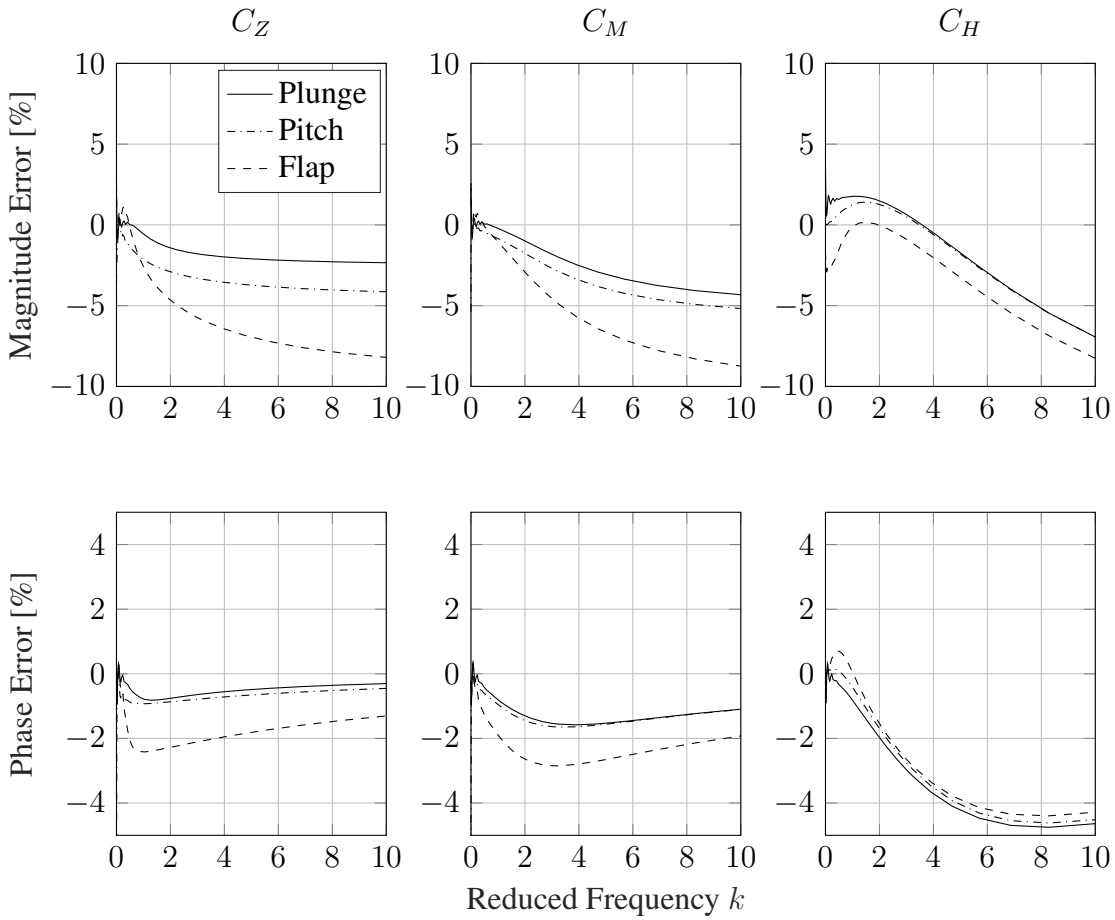

Figure 4: Frequency response error of the linearized continuous time UVLM in magnitude and phase with respect to Theodorsen [15] for plunging, pitching and flap oscillatory motion.

Figure 4 shows the error in the frequency response of the linearized model (second model) with respect to the analytical solution for harmonic plunging, pitching and flap motion and reduced frequencies ranging from 0 to 10. It can be seen that the error in the coefficients is especially high for flap oscillatory motion. Also the error in the hingemoment coefficient is larger than the overall airfoil pitching moment and vertical force coefficient. A possible cause is the discrete manner of panel methods. Linear downwash distributions as they occur for pitching and flap motion are approximated panel-wise constant. Since integrated values do not provide enough information, the chordwise distribution of the forces is discussed next to further understand the origin of the errors.

3.1.2 Unsteady Pressure Distribution

The expressions used for the analyses in this paper have been taken from Kier who summarized the derivation of analytical expressions in [16]. The unsteady pressure distribution of the UVLM is computed by looking at the response of single panels to harmonic plunging, pitching and flap motion at specified reduced frequencies.

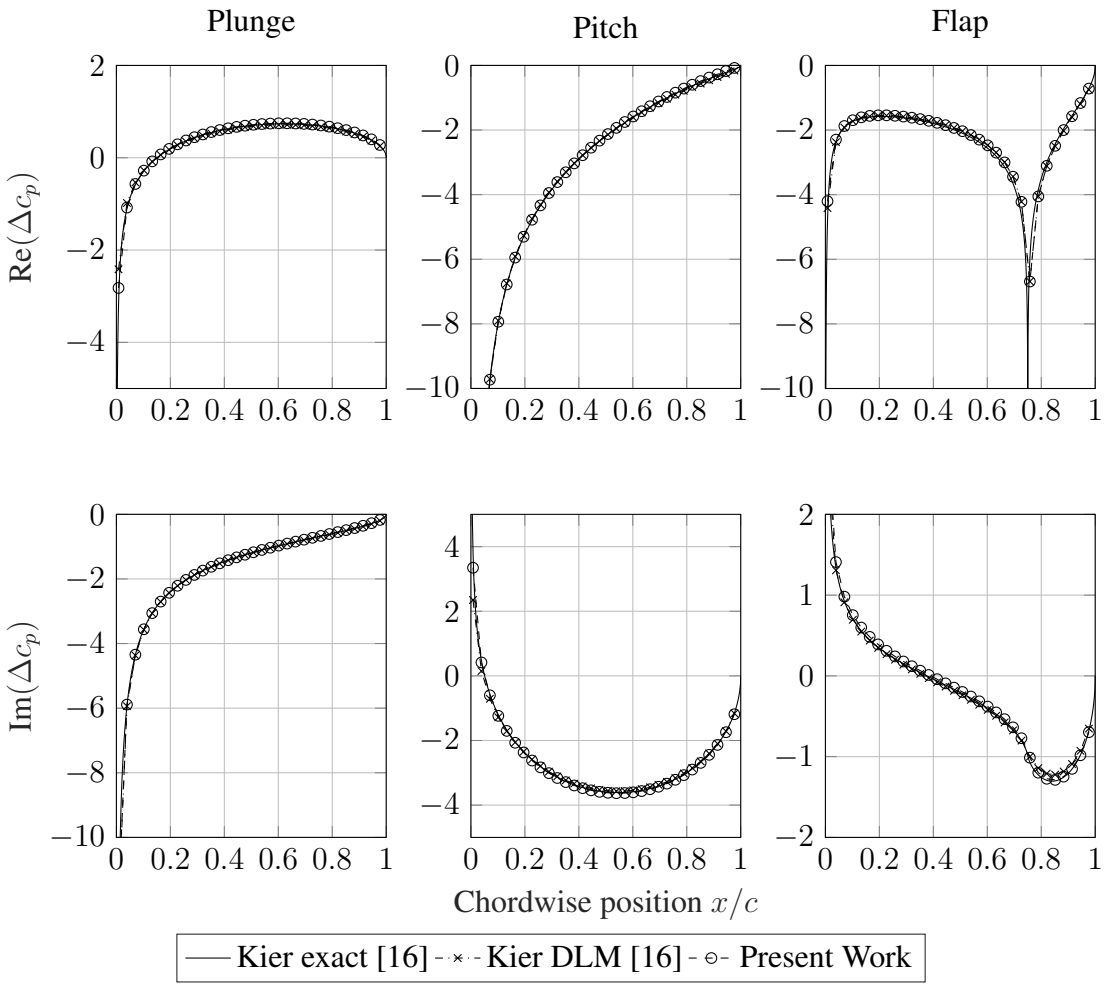

Figure 5: Real and imagniary part of the unsteady pressure distribution for a frequency of $k = 0.5$.

Figure 5 shows the real and imaginary parts of the unsteady pressure distribution for a moderate reduced frequency of $k = 0.5$. The overall characteristics are in excellent agreement. This counts for the UVLM as for the DLM. A closer look at the magnitude and phase difference is needed in order to make further conclusions.

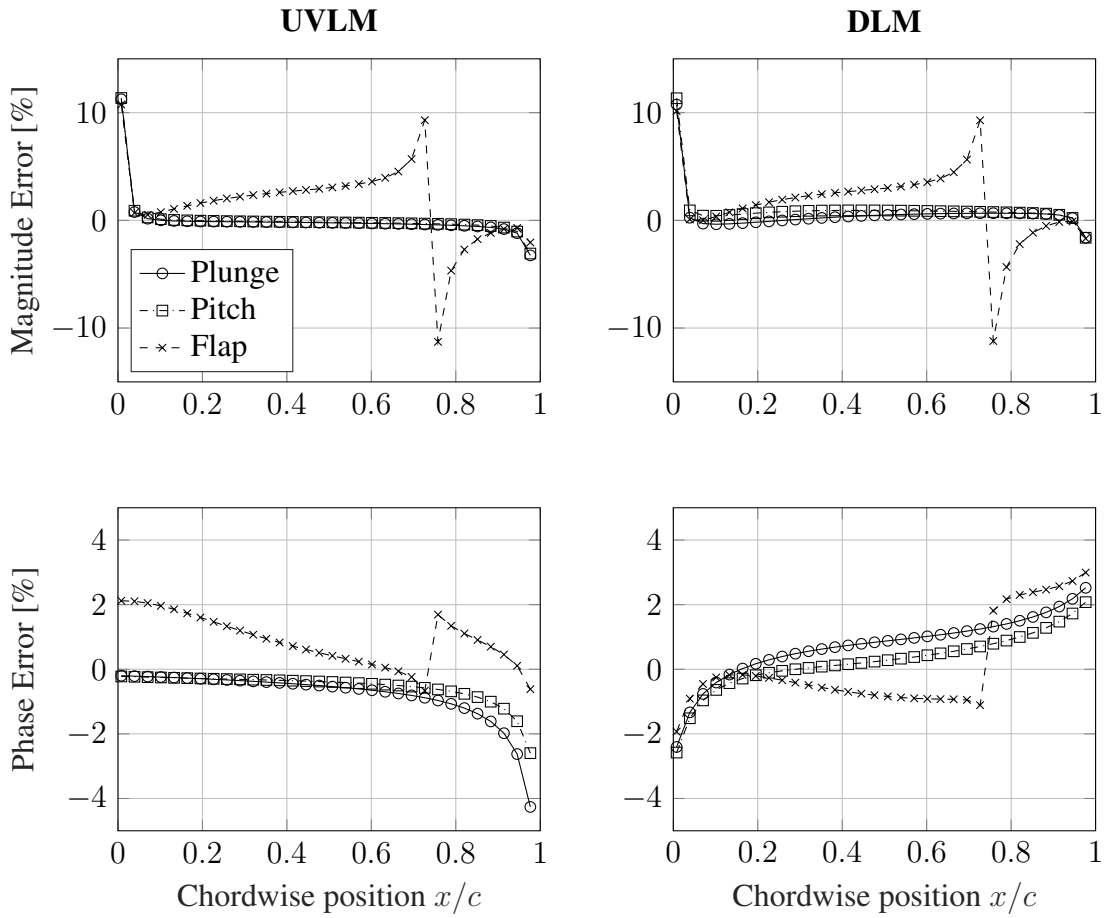

Figure 6: Magnitude and phase difference in the unsteady pressure distribution of the UVLM (left) and the DLM(right, [16]) compared to the exact method presented in [16] for a reduced frequency of $k = 0.5$.

Figure 6 shows the error in magnitude and phase which reveals that the biggest difference for plunging and pitching motion occurs at the leading and trailing edge. For flap oscillatory motion, a greater difference in magnitude can be also found near the hingeline. One reason for the differences is the discrete nature of the UVLM and the DLM. The height and position of the suction peaks (see Figure 5) at the the leading edge and control surface hinge position can not be resolved correctly. This explains the errors of the UVLM in magnitude and phase of the integrated coefficients for flap motion. The errors in magnitude and phase are comparable between the UVLM and the DLM for a reduced frequency of $k = 0.5$.

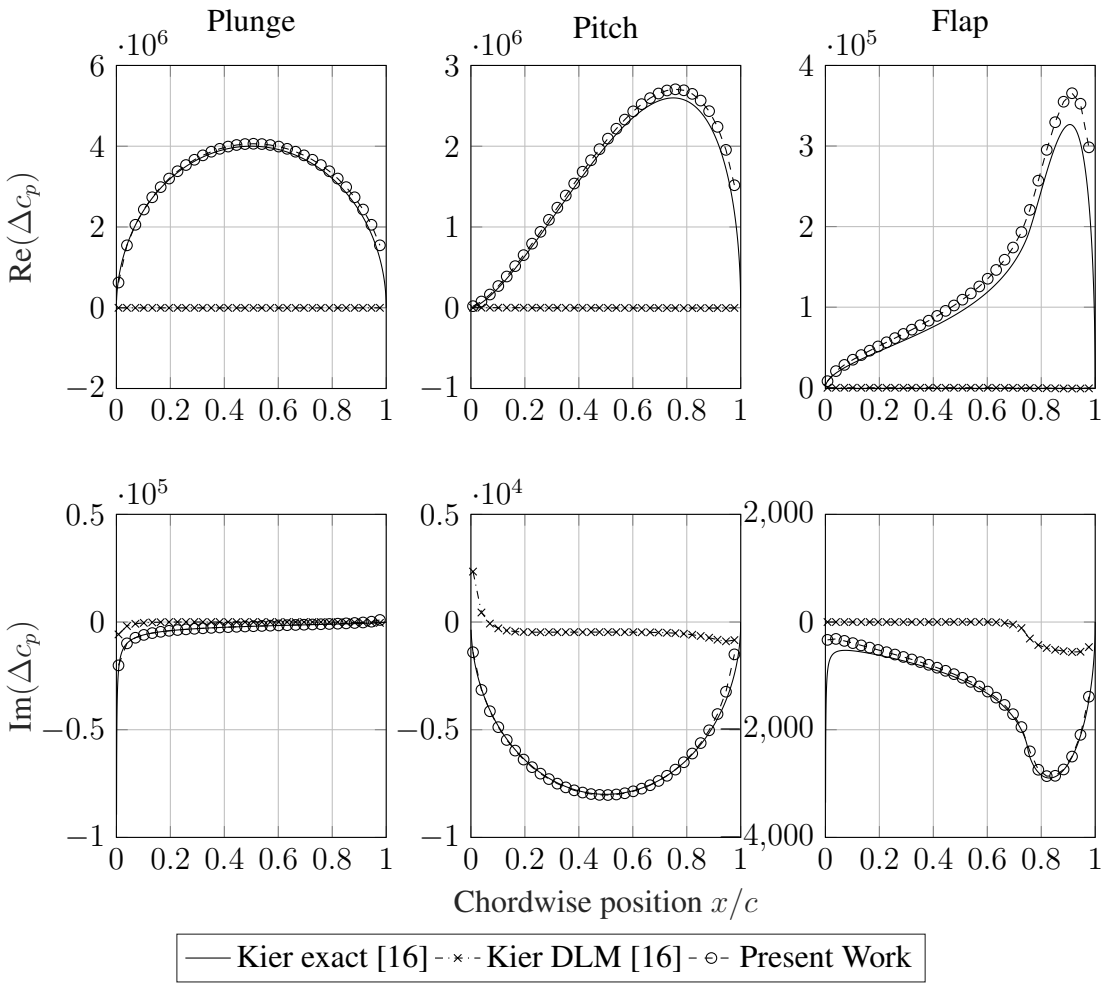

Figure 7: Real and imagniary part of the unsteady pressure distribution for a reduced frequency of $k = 1000$.

Figure 7 shows the unsteady pressure distribution for an extremely large reduced frequency of $k = 1000$. Of course, such a high frequency has no practical importance. Remarkable is the performance of the UVLM compared to the results produced by Kier with the DLM for high reduced frequencies and the same chordwise discretization. While the DLM "breaks down completely" [16] and is not capable of representing any of the high frequency characteristics, the UVLM shows quite good results for all types of motion and all coefficients.

3.1.3 Influence of the Chordwise Discretization

As already mentioned, a finer discretization can reduce the errors introduced by panel-wise constant approximations of forces and boundary conditions. Thus, a grid dependency study is carried out varying the chordwise discretization from 10 to 100 panels on the wings surface. The wake panels are adjusted accordingly so that the length of the panels in the wake always matches the length of the panels on the wing surface.

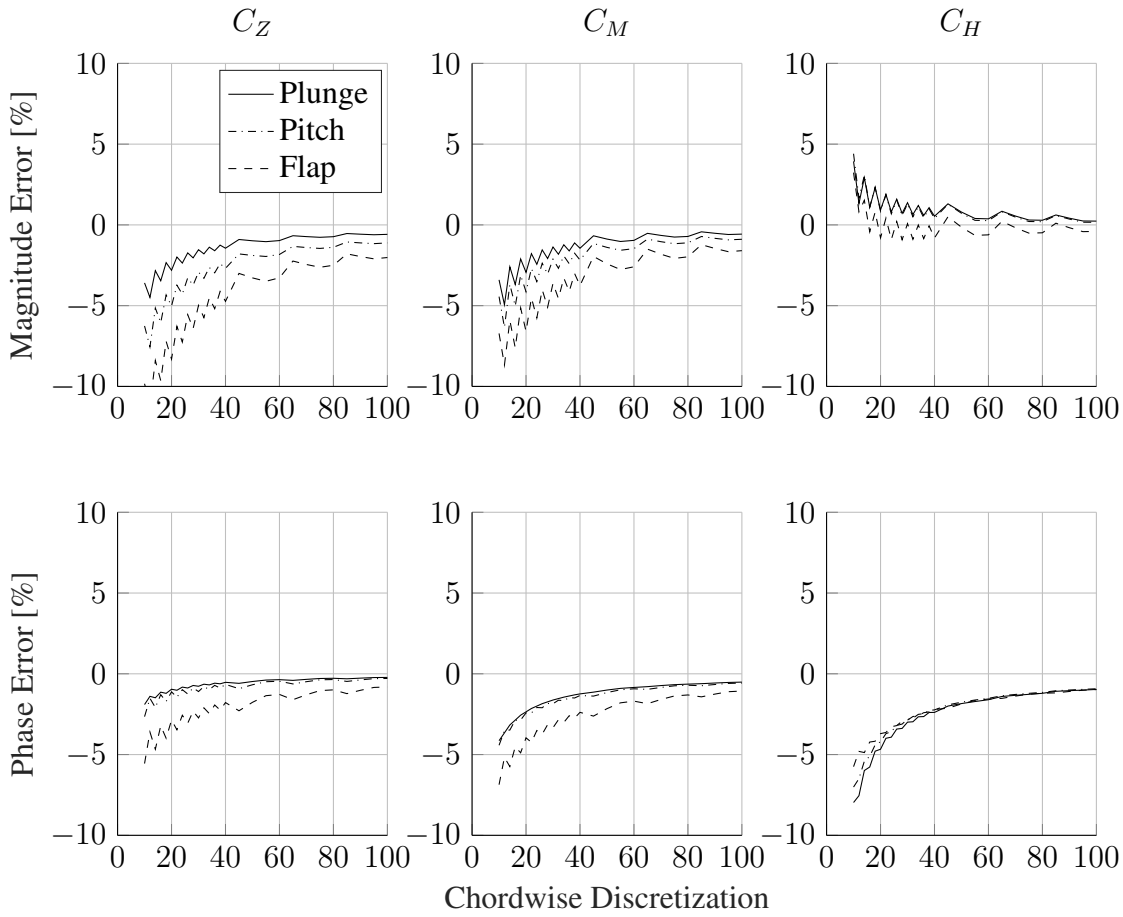

Figure 8: Convergence behaviour of the integrated coefficients (left: vertical force coefficient C_Z; middle: pitching moment coefficient C_M; right: flap hinge moment coefficient C_H) with respect to chordwise discretization (number of panels in chord direction) for a reduced frequency of $k = 3$.

Figure 8 shows the magnitude and phase error of the integrated values at a reasonable reduced frequency of $k = 3$ for various chordwise discretizations. The results show that for a reduced frequency of $k = 3$ a minimum discretization of $\sim$40 panels is needed to keep the error in all coefficients lower than 5%. As the highest error occurs for flap oscillatory motion and hinge moment coefficient, a finer discretization of the control surface compared to the rest of the wings surface and the wake could be a way to find a compromise between large model order and overall accuracy. Since the error is not approaching exactly zero the influence of the wake length is analyzed next.

3.1.4 Influence of the Wake Truncation Distance

The UVLM requires the modeling of the wake. Since the wake is theoretically infinite, the wake has to be truncated in order to realize a model with a finite number of states. In the following, the truncation distance is varied ranging from 1 to 65 chord-lengths c. By computing the error of the coefficients at various wake-lengths to the coefficients calculated using the maximum wake-length, the relative error is obtained. Figure 9 shows the maximum occurring error (max(err$_{C_Z}$,err$_{C_M}$,err$_{C_H}$)) in dependency of the wake truncation distance.

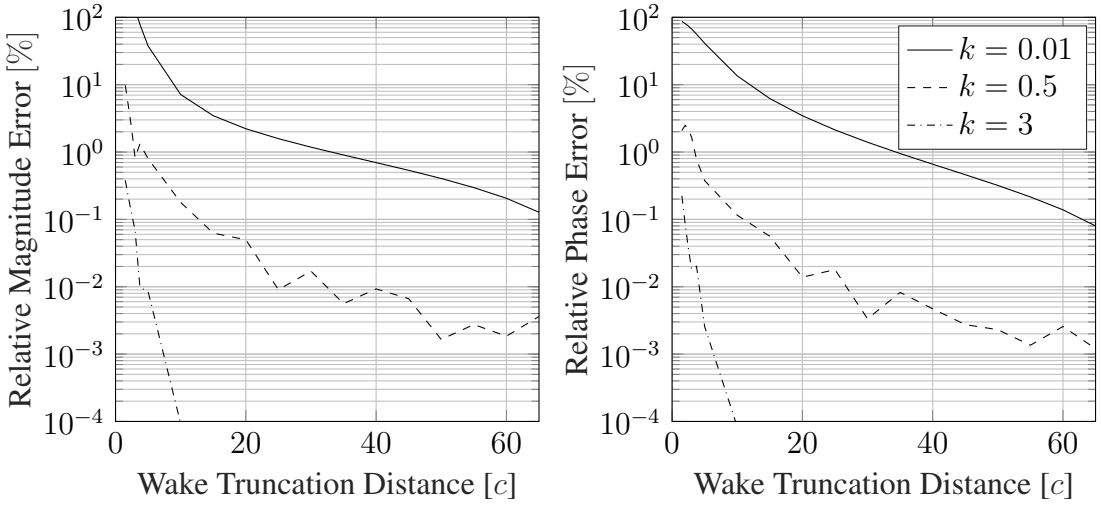

Figure 9: Influence of wake truncation distance (in multiples of chord lengths c) on maximum occurring relative difference (max(err$_{C_Z}$,err$_{C_M}$,err$_{C_H}$)) between the UVLM and Theodorsen [15] in magnitude (left) and phase (right).

The results in Fig. 9 show that a wake truncation distance of $40c$ is required to keep the error in all derivatives lower than 1 %. This requirement is strongly driven by low frequency dynamics. For higher frequencies, the wake truncation distance has only little influence on magnitude and phase of the coefficients.

3.2 Induced Drag Calculations using the Nonlinear Model

The calculation of the unsteady drag within the UVLM is compared to analytical results for the leading edge suction force formulated by Garrick [17]. Garrick formulated the leading edge suction force for harmonic plunging and pitching motions. Simpson et al. [12] summarized the formulation and compared a discrete time-stepping version of the UVLM to Garrick's results. The summary presented by Simpson et al. is used for the generation of the following reference results.

The UVLM model with nonlinear force computation (first model, see Ch. 2.4) is used for comparison. Time domain plunging ($h = h_0 \sin(\omega t)$) and pitching ($\alpha = \alpha_0 \sin(\omega t)$) simulations are carried out for reduced frequencies of $k = 0.1, 1$ and 3 with plunging amplitudes of $h_0 = \frac{0.01c}{k}$ and a pitching amplitude of $\alpha_0 = 1^\circ$ for all reduced frequencies. The comparison includes results from a classical discrete time stepping UVLM which is part of dAEDalus [8]. The discretization and wake length are chosen as in the simulations with the linearized model (see Ch. 3.1). Figure 10 shows the results for the induced drag coefficient C_d in plunging and pitching motion plotted against the effective angle of attack α_{eff} (with $\alpha_{\text{eff}} = \tan^{-1}(\frac{h_0}{|V_\infty|})$ for plunging motion).

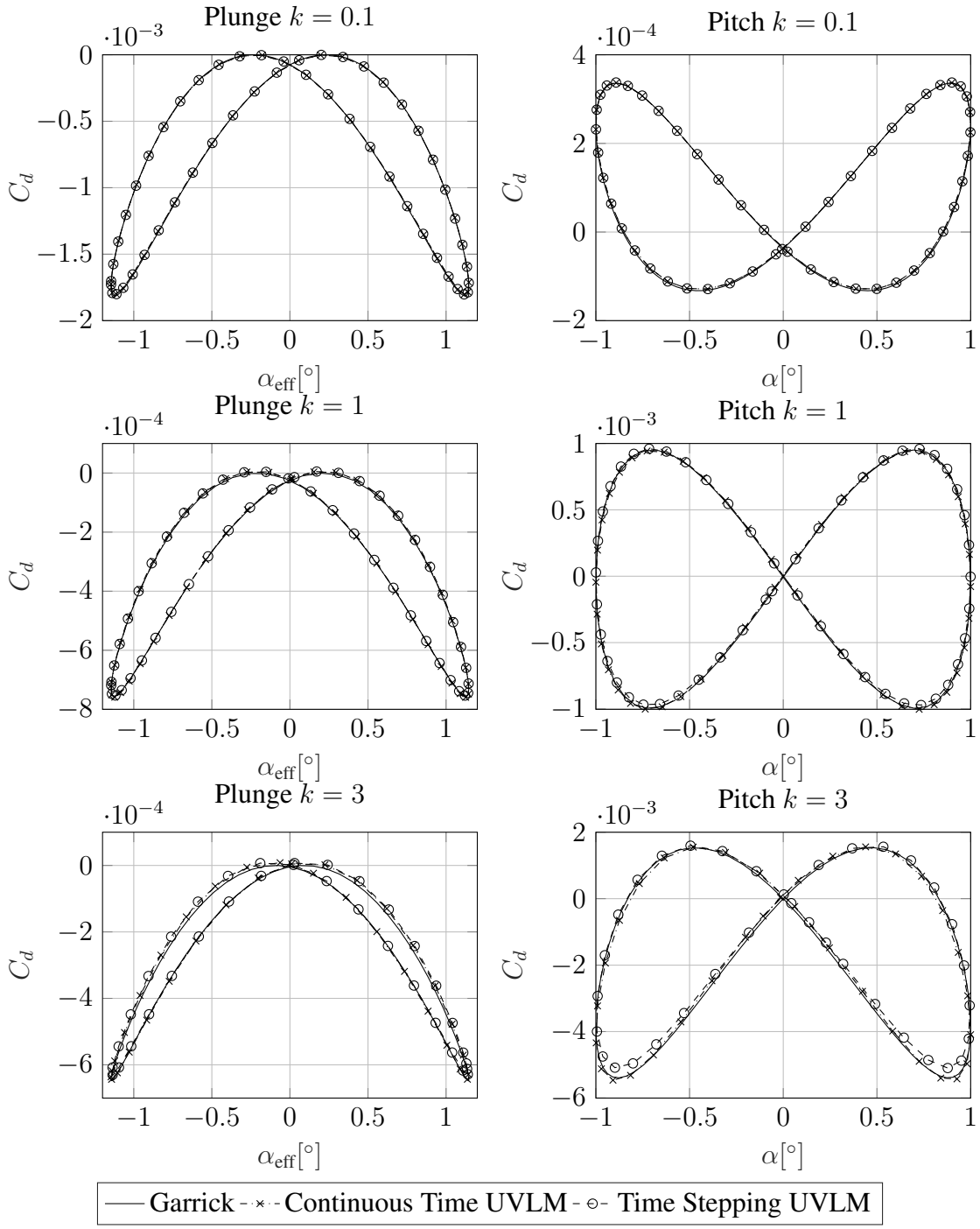

Figure 10: Unsteady induced drag for reduced frequencies of $k = 0.1$ (top), $k = 1$ (middle), $k = 3$ (bottom), oscillatory plunging (left) and pitching (right) motion over angle of attack (α_{eff} for plunge; α for pitch).

The results show that the proposed continuous time UVLM is accurately predicting the induced drag calculated by the analytical formulation. It can be seen that the drag for plunging motion is always negative (propulsive force). For harmonic pitching, the net force direction changes with the reduced frequency. As expected, the performance of the time stepping formulation regresses with increased frequency since the maximum spatial-temporal distance which can be resolved by the chosen time-wise discretization is limited. The continous time formulation on the other hand has neither a lower limit nor a discretization dependency for the time-step of the

simulation. Thus, the continous time UVLM produces better results at high frequencies at the same chordwise discretization than the classical time-stepping approach.

4 CONCLUSIONS AND OUTLOOK

An extension for the continuous time unsteady vortex lattice method has been presented enabling aerodynamic modeling for arbitrary motion and control surface deflection including induced drag calculation. The extension includes a formulation of the boundary conditions for arbitrary three-dimensional motion and control surface rotation. Furthermore the calculation of unsteady induced drag by a nonlinear extension of the force computation has been outlined. The nonlinear state space realization was explained and a linearized version has been presented. For validation of the method, simulations of both, the nonlinear as well as the linearized model have been carried out. The results for integrated coefficients and pressure distributions of 2D airfoils are in excellent agreement with the analytical methods. Furthermore the proposed method shows advantages in predicting unsteady aerodynamic forces of high frequency motion compared to the DLM and the classical time-stepping UVLM.

In general, it can be said that the unsteady vortex lattice method is a powerful tool for modeling of incompressible and inviscid unsteady aerodynamics. The continuous time formulation in particular can be used to decrease the computational costs for aeroelastic simulations. Current studies found that the number of states can be drastically reduced using model order reduction techniques [18]. In the future, the model will be used within dAEDalus for aeroelastic stability and performance analysis. The possibility of calculating unsteady loads without the need of approximations for time-domain simulation makes the method especially useful within aeroservoelastic optimization algorithms. Other models formulated in time domain (for example sensor and actuator models or control laws) can be easily integrated. Furthermore, the nonlinear aerodynamic state space formulation is suitable for the integration of further nonlinear aerodynamic correction models (e.g. stall models).

5 REFERENCES

[1] Kier, T. (2005). Comparison of unsteady aerodynamic modelling methodologies with respect to flight loads analysis. In *AIAA Atmospheric Flight Mechanics Conference and Exhibit*. Reston, Virigina: American Institute of Aeronautics and Astronautics. ISBN 978-1-62410-055-0. doi:10.2514/6.2005-6027.

[2] Murua, J., Palacios, R., and Graham, J. M. R. (2012). Applications of the unsteady vortex-lattice method in aircraft aeroelasticity and flight dynamics. *Progress in Aerospace Sciences*, 55, 46–72. ISSN 03760421. doi:10.1016/j.paerosci.2012.06.001.

[3] Hall, K. C. (1994). Eigenanalysis of unsteady flows about airfoils, cascades, and wings. *AIAA Journal*, 32(12), 2426–2432. ISSN 0001-1452. doi:10.2514/3.12309.

[4] Gologan, C. and Schneider, G. (2001). New aerodynamic approach for manoeuver simulation including dynamic loads. *DGLR-Jahrbuch*, (DGLR-2001-067).

[5] Mauermann, T. (2010). *Flexible Aircraft Modelling for Flight Loads Analysis of Wake Vortex Encounters*. Dissertation, Technische Universität Braunschweig, Braunschweig.

[6] Mohammadi-Amin, M., Ghadiri, B., Abdalla, M. M., et al. (2012). Continuous-time state-space unsteady aerodynamic modeling based on boundary element method. *Engineering Analysis with Boundary Elements*, 36(5), 789–798. ISSN 09557997. doi: 10.1016/j.enganabound.2011.12.007.

[7] Noud P.M. Werter, Roeland De Breuker, Mostafa M. Abdalla. Continuous-time state-space unsteady aerodynamic modelling for efficient aeroelastic load analysis, 1–12. doi: 10.1002/9781118266892.ch1.

[8] Seywald, K. (2016). *Impact of Aeroelasticity on Flight Dynamics and Handling Qualities of Novel Aircraft Configurations*. Dissertation, Technische Universität München, München.

[9] Katz J. and Plotkin, A. (1991). *Low-Speed Aerodynamics*. New York: McGraw-Hill. ISBN 0-07-050446-6.

[10] Murray, R. M., Li, Z., and Sastry, S. (1994). *A mathematical introduction to robotic manipulation*. Boca Raton: CRC Press. ISBN 0849379814.

[11] Drela, M. (1999). Integrated simulation model for preliminary aerodynamic, structural, and control-law design of aircraft. In *40th Structures, Structural Dynamics, and Materials Conference and Exhibit*. Reston, Virigina: American Institute of Aeronautics and Astronautics. doi:10.2514/6.1999-1394.

[12] Simpson, R. J. S., Palacios, R., and Murua, J. (2013). Induced-drag calculations in the unsteady vortex lattice method. *AIAA Journal*, 51(7), 1775–1779. ISSN 0001-1452. doi: 10.2514/1.J052136.

[13] Pesmajoglou, S. D. and Graham, J. (2000). Prediction of aerodynamic forces on horizontal axis wind turbines in free yaw and turbulence. *Journal of Wind Engineering and Industrial Aerodynamics*, 86(1), 1–14. ISSN 01676105. doi:10.1016/S0167-6105(99)00125-7.

[14] Stanford, B. K. and Beran, P. S. (2010). Analytical sensitivity analysis of an unsteady vortex-lattice method for flapping-wing optimization. *Journal of Aircraft*, 47(2), 647–662. ISSN 0021-8669. doi:10.2514/1.46259.

[15] Theodorsen, T. (1935). General theory of aerodynamic instability and the mechanism of flutter. *NACA Report 496*.

[16] Kier, T. M. (2011). An integrated loads analysis model including unsteady aerodynamic effects for position and attitude dependent gust fields, 1–12. doi: 10.1002/9781118266892.ch1.

[17] Garrick I. E. Propulsion of a flapping and oscillating airfoil. *NACA Report 567*.

[18] Gillebaart, E. and de Breuker, R. (2015). Reduced-order modeling of continuous-time state-space unsteady aerodynamics. In *53rd AIAA Aerospace Sciences Meeting*. Reston, Virginia: American Institute of Aeronautics and Astronautics. ISBN 978-1-62410-343-8. doi:10.2514/6.2015-0260.

COPYRIGHT STATEMENT